

MSEC_ICM&P2008-72195

ESTIMATION OF TEMPERATURE DISTRIBUTION IN SILICON DURING MICRO LASER ASSISTED MACHINING

Kamlesh J. Suthar[#]

Mechanical and Aeronautical Engineering
Western Michigan University
Kalamazoo, MI-49008, USA

Lei Dong

Condor USA, Inc.
8318 Pineville-Matthews Road, Suite 276
Charlotte, NC-28226

John Patten^{*}

Manufacturing Engineering Department
Western Michigan University
Kalamazoo, MI-49008, USA

Hisham Abdel-Aal

Department of General Engineering
University of Wisconsin at Platteville
Platteville, WI- 53818, USA

ABSTRACT

Silicon is machined using a diamond tool and the process is assisted with an IR Laser for the purpose of heating and thermal softening the work piece material. The laser beam passes through the tool and into the work piece, where the material is both thermally heated (by the laser) and mechanically deformed (by the tool). The laser is used to increase the work piece temperature (up to the softening temperature of silicon, about 500-800°C [10]), while the tool deforms and cuts the heated and softened silicon in the ductile regime, without producing cracks. This hybrid laser assisted machining process results in a smooth plastically deformed surface and extends the life of the diamond tool when cutting a hard and abrasive material, e.g. silicon. Scratch tests were done using the micro laser assisted machining method with diamond tools, which demonstrated enhancement in the depth of cut from 60 nm to 120 nm with (a 2x increase in depth of cut, at a constant load) while the cutting speed varied from 0.305 mm/sec to 0.002 mm/s. An analytical and numerical method was used to estimate the temperature rise in the vicinity of the diamond tool due to laser irradiation and absorption by the silicon work piece. It is assumed that the layer of silicon that absorbs the heat from the laser radiation is silicon II. Silicon II is a metallic phase of silicon, commonly referred to as the beta-tin structure, formed by a high pressure phase transformation (HPPT). In this context, the analytical

and numerical models are solved using the heat conduction equation for semi-infinite solid over time with a Gaussian laser beam intensity distribution. The temperature rise for different cases (laser intensity, depth of cut, cutting speed, etc.) was modeled using point, and plane heat source method with Gaussian intensity distribution. These results are discussed in detail to estimate the temperature distribution while machining.

1 INTRODUCTION

To achieve an atomic level surface smoothness and to extend the tool life, a novel micro laser assisted machining (μ -LAM) technique, is employed. In this technique, silicon (or other semiconductor/ceramic materials) is machined using a diamond tool with the assistance of an IR laser that increases the temperature of silicon up to its thermal softening point. Scratch tests done using laser μ -LAM technique, where the thrust or normal force is applied using a modified stylus profilometer; the formation of silicon II is achieved via the HPPT. Complete details of this experimental procedures and results can be found in the dissertation work of Dong [3].

An analytical and numerical approach is adopted to estimate the temperature rise in the vicinity of the diamond tool due to the laser absorption by the different phases of silicon (silicon I and silicon II, where silicon I is the covalent – semiconductor phase). In this context, the analytical models are solved using the solution based on Hou et. al. [5] and [2].

#kamleshkumar.suthar@wmich.edu

*john.patten@wmich.edu 1-(269) 276-3246 (O) 1-(269) 276-3257 (F)

Hou et. al. [5] integrated a point heat source in the heat conduction equation for an infinite solid over time. The commercially available MatLab software is used to solve these analytical models.

2 NOMENCLATURE

k	Thermal Conductivity W/cm/K
t	Time in sec
erfc	Complementary error function
α	Thermal Diffusivity cm ² /sec
r	Reflectivity
ρ	Density g/cm ³
R	Distance between laser and some point M in space
	$= \sqrt{x^2 + y^2 + z^2}$
X	$= x - v \cdot t =$ distance between moving laser and some point M in space
v	Velocity in cm/s
Peak intensity	$I_o = \frac{P}{A_o}$
Effective spot area	$A = \pi r_x r_y$
Average radius	$r = \sqrt{r_x r_y}$
Eccentricity factor	$\beta = \frac{r_x}{r_y}$

3 PROBLEM DESCRIPTION

This paper is focused on estimating the temperature of silicon during μ -LAM based on our previous experimental work [3]. A novel approach of heating is adopted, wherein an IR-Laser is coupled and transmitted to a diamond tool with a fiber optic. A 1480nm wavelength, 400mW IR laser is fed through 5 μ m radius diamond tool to achieve thermal softening due to absorption of the laser energy by the silicon work piece. Figure 1 shows the mechanism of the material removal process. In this research, we have used a standard 4 inch diameter single crystal silicon (100) p-type wafer. Caused by mechanical loading, the material beneath the diamond tool undergoes a high pressure phase transformation (HPPT) change and converts the semiconducting silicon into the metallic phase of the silicon [3]. Covalent silicon (Si-I) is mostly transparent to this laser wavelength, while the metallic, high pressure, phase is opaque. Thus, no direct heating of the Si-I by the laser occurs and preferential heating of Si-II is achieved [3]. Irradiation by the laser increases the temperature of the silicon, up to its thermal softening temperature (500-800 °C). This situation involves various mechanisms to produce the temperature rise. Since, two surfaces are sliding against each other (diamond tool and silicon work piece) and the tool is exerting force on the silicon, this is also a tribological problem. However, the contribution in temperature rise due to tribological friction is only 3-4 °C at relatively slow cutting

speeds used in the previous experiments [Annex A]. This temperature rise is negligible compared to the laser absorption; which has been confirmed using the equation (4), as shown in section 4.3.

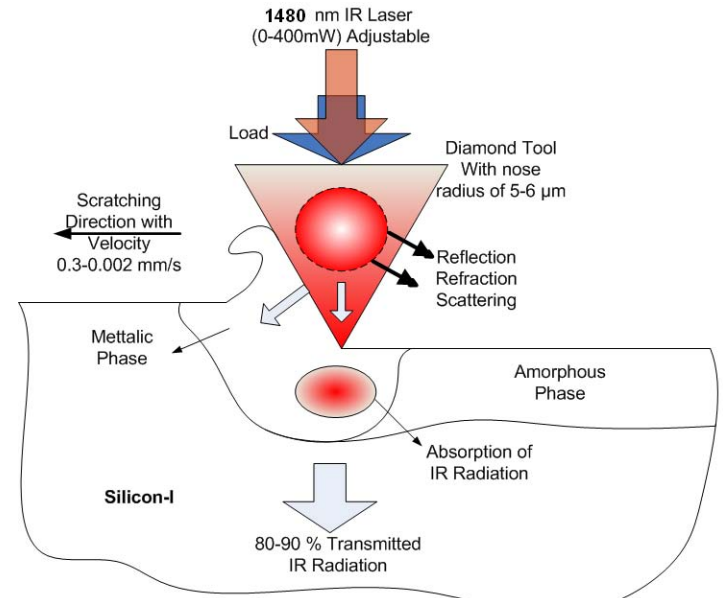


FIGURE 1: MICRO LASER ASSISTED MACHINING MECHANISM SCHEMATIC.

Several different tests were performed previously, e.g. scratch test, scratch and stay test; and each were analyzed analytically. The diamond tool, approximately 5 μ m tip radius and 250 μ m base diameter, is fastened to a laser fiber ferrule with UV cured epoxy; the fiber itself is 10 μ m in diameter. Approximately, 70% of the irradiated energy is concentrated within a 4 μ m diameter area at the center of the beam [3]. This is crucial information with respect to estimating the power input to the work piece. The laser power was measured and compared with and without the diamond tool and is shown in figure 2. This graph shows slightly greater than a 50 % reduction in available output laser power due to attachment of diamond tool (due to reflection and scattering losses). Therefore, about 150 mW of usable laser power is achieved using a 400mW laser.

We have previously performed scratch tests to determine the thermal properties of the silicon II (refer to table 1) with respect to temperature; more detail can be found elsewhere [1]. Table 2 shows the experimental parameters that are used in this paper.

Ductile regime machining of silicon, without brittle fracture, is restricted to small depths of cut and feeds. Typical depth of cut is 100 nm, with a feed of 1 μ m/rev for precision machining of silicon. Figure 3 shows the effect of laser power on the depth of cut and the results for changes in the cutting speed. The depth of cut is measured by an AFM. As the cutting speed decreases or as the laser power increases, the depth of cut also increases. The maximum increase, up to a factor of

two (2x) at a fixed normal or thrust force which leads to a conclusion that the laser effectively increases the temperature of the specimen to achieve thermal softening.

TABLE 1: SILICON-II PROPERTIES

Temperature (K)	Thermal Conductivity of metallic Si-II W/cm/K
300	0.0025
400	0004
500	0.0055
600	0.0075
700	0.0125
800	0.0165
900	0.025

TABLE 2: PARAMETERS USED IN EXPERIMENT

IR Laser	
Wavelength	1480nm
Laser Power (max)	400mW
Power at Diamond Tip	140mW
Photon energy	0.9 eV
Reflectivity of Si-II	0.9
Diamond tool	
Diameter of tip	5 μ m
Thermal conductivity	900-1200 W/m/K
Silicon	
Specific heat	0.7J/g/K
Density	2.33 g/cm ³

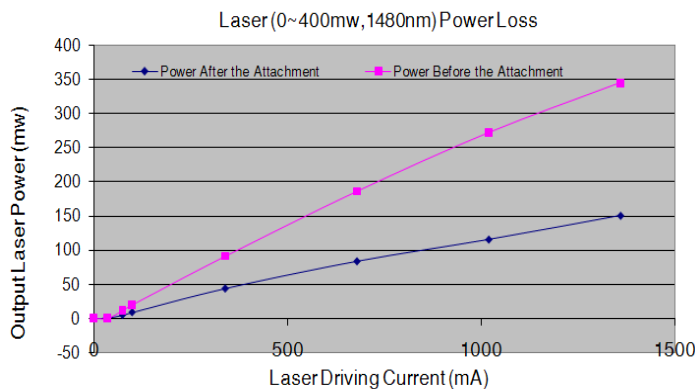


FIGURE 2: EFFECT OF DIAMOND ATTACHMENT ON POWER OUTPUT

The formation of silicon-II underneath the diamond tool is confirmed using Raman spectroscopy [3]. It is difficult to measure or estimate the temperature experimentally because of the small feature size (nanometers to micrometers in extent) and the complexity of the material properties; for instance the material properties of the high pressure metallic phase of silicon, Si-II, are not well known.

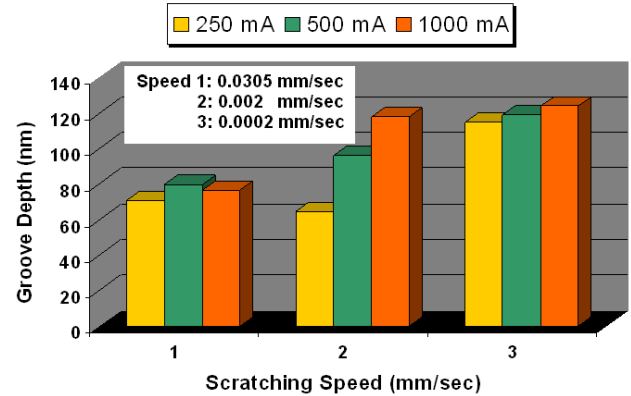


FIGURE 3: EFFECT OF SCRATCHING SPEED AND LASER POWER ON DEPTH OF CUT [3]

IR images were taken to reveal the thermal condition of the silicon beneath the diamond tip. Details of IR images can be found in annex-B as found in reference [3]. The black line in figure 10 represents the interface between tool and silicon work piece. Also, the load versus penetration depth can be related to a hardness value, and this is correlated back to a temperature via a hardness-temperature relationship [10].

The diamond tip, with a preload of 40mN, was set on the silicon wafer and remained stationary. The silicon wafer, which is fixed on the load cell, is moved at by a linear motor. After the diamond tip is set on the wafer with the applied load, the movement of the wafer generates the scratch. The scratching stops when the diamond tip reaches the edge of the wafer, where the focal point of the IR camera is preset. The diamond tip stays at the end of the scratch groove for a period of 20 seconds with the laser running at its maximum output power. The IR camera records the stationary diamond tip for the entire 20 second time period while the loading is maintained along with the laser irradiation. The IR thermal images that represent the changing heat distribution of the diamond tip and the adjacent silicon are shown in figures 10 to 15 (refer to the appendix). The x and y axes in these figures are pixel numbers. The color scale in these images is the relative amount of photon energy (cm⁻¹) in each pixel which is not calibrated. The camera, for each image frame, automatically adjusts this scale. Therefore, the photon energy distribution is not directly comparable from one image to the next, as the scale changes with each image. In the last 5 seconds, the silicon under the diamond tip indicates significant thermal changes, as shown in figures 10 to 15. These figures represent sequential images or stages that occur during the final 5 seconds of heating. After 15 seconds, a zone in the silicon (estimated depth of 200nm below the silicon surface and about 100 nm thick) beneath the diamond tip appears to radiate and the photon intensity in this area progressively increases (from Figure 10 though 15). The heated area gradually increases in extent and relative intensity. By the end of the measuring period (20 seconds), the highest photon intensity zone has shifted to the heated area under the diamond

tip. The photon energy is not continuous from the diamond tip to the heated zone of the high pressure metallic phase of silicon, which indicates that this is not simply a conduction related phenomenon. If the diamond was being heated also, then the observed hot zone would be continuous from the diamond tip down into the silicon. The cold spot (representing a discontinuity) between the diamond tip and the heated silicon, refer to Figures 10 and 13, indicates that there is another phenomenon involved, i.e. the heating of the high pressure metallic phase of silicon, which is confirmed by the measurement of hardness, reduced from 12GPa to 6GPa [3]. Also noteworthy, is that the surrounding bulk silicon (covalent silicon material) does not seem to respond to the IR laser. This is expected as covalent silicon is transparent in the IR and the surrounding bulk silicon is not heated by the IR laser. There is also a lack of IR thermal emission or scattering of the laser beam from the surrounding silicon. Thus, it can be concluded that the covalent silicon does not appreciably interact with the IR laser beam and temperature increases beneath the tool which leads to softening temperature.

The evidence, to estimate the temperature rise in silicon, the problem is analyzed by an analytical and numerical method which is given in the following sections. First of all the problem is solved for tribological approach to evaluate the temperature rise due to friction with respect to velocity. These results are not discussed here, because the contribution of the temperature rise due to friction is negligible which, further confirms the temperature rise is a product of the laser not just the mechanical loading.

4 ANALYTICAL MODEL

4.1 Governing Equations for Temperature Profile

The equations used in this modeling are based on solution of conduction equation using green functions method [5-7]. Parameters taken for this research work is tabulated as in table-2. During modeling it is seen that results of modeling at constant thermo-physical properties at initial temperature or at final temperature, are not convincing, because taking constant properties at low temperature or at high temperature; the equation/model over predicts or under predicts the temperature rise. Therefore, properties at an intermediate temperature are taken in order to obtain more convincing results. This assumption was confirmed by the methods reported in [5-7]. In the following analysis, we have taken the thermo-physical properties at some intermediate temperature. Moreover, due to HPPT silicon-I convert into Si-II forming a layer of 100nm -1 μm layer on top surface, which create composite layered structure of the silicon-I and II. Considering intermediate properties 0.03 W/cm/K thermal conductivity is taken wherever it is necessary. For all analytical calculation the thermo physical properties are calculated considering composite silicon as mentioned earlier. Following sections discuss the equation used for analysis in different cases of machining e.g. scratch test, scratch and stay test and machining. Stationary Point Heat Source

Following equation (1) shows the point heat source temperature which is used to calculate the temperature rise in the scratch and stay test. The temperature rise was around 800oC.

$$T = \frac{q(1-r)}{2\pi kR} \operatorname{erfc}\left(\frac{R}{\sqrt{4\alpha t}}\right) \quad (1)$$

This is for semi-infinite solid; this equation is reduced form of an infinite (work piece) solution, which has half of this temperature compared to the infinite solution. [5]

$$\alpha = \frac{k}{\rho C_p}$$

Where,

Equation 1 is derived from the instantaneous point heat source [5] the numerical form of the equation is given as below which is integrated over time. [5]

$$T = \frac{2q(1-r)}{C_p \rho} \frac{1}{4\pi\alpha^{3/2}} \int_{\tau=0}^{\tau=t} \frac{d\tau}{\tau^{3/2}} e^{\left(-\frac{x^2+y^2+z^2}{4\alpha\tau}\right)} \quad (2)$$

To estimate the moving scratching test above equation is modeled with respect to time for temperature profile. Equation 2 is similar to the equation 1 which is solved numerically to compare the solution for moving point heat source.

Considering plane contact between tool and work-piece, an analytical equation of moving plane heat source is modeled to estimate the heat generation during machining. The estimated temperature rise is negligible for the given load of 40mN.

4.2 Moving Plane Heat Source

Moving plane heat source equation is modeled in Matlab to estimate the tribological temperature rise during the scratch test.

$$T = \frac{q(1-r)}{2\pi kR} \exp\left(-\frac{R+X}{2\alpha v}\right) \quad (3)$$

Equation 3 have two terms, the first term is temperature term and the second term is non-dimensional term which depends on thermo-physical properties and velocity. The second term is asymmetric function with varying x, which has the $Rv/2\alpha$ term gives higher asymmetry with higher values of R or v or α . While the first term has symmetric function, therefore, if this term is much higher than the second term, it gives us low variation with respect to the distance and this is what happening in our case.

Equation of moving point heat source for semi-infinite solid is as below, [5].

$$T = \frac{2q(1-r)v}{16k\alpha\pi^{3/2}} e^{\left(-\frac{Xv}{2a}\right)} \int_0^{\frac{v^2 t}{4a}} \frac{d\varpi}{\varpi^{3/2}} e^{\left(-\varpi\left(\frac{u^2}{2a}\right)\right)} \quad (4)$$

Where, $\varpi = \frac{v^2 t}{4\alpha}$ and $u = \frac{Rv}{2a}$

This equation is for tribological application in which rubbing motion generates the heat, considering the heat source at the interface. The integration part is similar to modified second kind Bessel function; however, it is not exactly Bessel function which is solved by numerical method. This solution gives higher temperature at higher speed, while for this research case; it produces higher temperature at lower velocities due to higher absorption. The analytical modeling in MatLab confirms very small temperature rise for given velocities and therefore, the results from this equation is not discussed for mentioned problem. This problem is unique in the following ways: the back conduction in diamond, the formation of Si-II whose properties are largely unknown and the laser energy absorption in Silicon-II.

Since the moving point heat source problem is for tribological application, it cannot be applied to mentioned problem. Please refer Annex-A for the results of the equation 4. Moving plane heat source equation mentioned above, assumes heat generation due to the friction. In the present case the heat is generated by irradiation of laser to the surface and absorption on the interface with the Gaussian profile of the beam. The following equation considers the Gaussian profile, moving plane heat source. Since this is being composite material, the aggregate thermo-physical properties are taken based on constant heat flux assumption.

4.3 Gaussian Profile Moving Plane with Laser Heat Source

The Gaussian profile Laser beam intensity equation is given by following equation [9]

$$I_{x,y} = I_o \exp \left[- \left(\left(\frac{x}{r_x} \right)^2 + \left(\frac{y}{r_y} \right)^2 \right) \right]$$

$$T(x,y,z) = \frac{Q(1-r)}{\pi^{3/2}k} \int_0^{\infty} f(u) du \quad (5)$$

Where,

$$f(u) = \frac{\exp \left(- \left[\frac{X + V\sigma u^2}{u^2 + 1/\beta} + \frac{Y^2}{u^2 + \beta} + \frac{Z^2}{u^2} \right] \right)}{\left[u^2 + 1/\beta \right]^{1/2} \left[u^2 + \beta \right]^{1/2}}$$

$$X = \frac{x}{r}, Y = \frac{y}{r}, Z = \frac{z}{r}, V = \frac{v}{r}, \sigma = \frac{r^2}{4\alpha}, Q = \frac{q}{r} \text{ and } u = \left(\frac{2\alpha t}{r^2} \right)^{1/2}$$

Above equations are solved numerically using commercially available mathematic software MatLab.

After careful evaluation of analytical solution the problem is simulated using FEM multi-physics software. Following section discusses the FEM formulation of the present problem.

5 FORMULATION OF FINITE ELEMENT ANALYSIS

The problem is also analyzed numerically using commercially available software with multi-physics capability, COMSOL 3.4. The properties of the materials are temperature dependent and implemented using a temperature function in heat conduction mode with the heat transfer module.

Silicon-II is sandwiched between the diamond tool and silicon-I and the absorption of the laser varies with depth of penetration. It is assumed that the maximum heat flux is absorbed in the middle of the silicon-II. 140 mW heat flux is taken with 80-90% reflectivity [4]. The absorption of 1480nm laser is approximately 10% [4, 11-12]. 5 μm beam radius is provided for the Gaussian beam profile. While the fiber diameter is 10 μm and the widest groove (scratch) produced by the diamond tool (for the loads and laser power investigated) was about 6 μm, therefore this value is used for our comparative analysis.

The results for the above analysis, including experimental observation and measurements, are discussed below.

6 RESULTS AND DISCUSSION

Figures 4 & 6 show the output of the moving plane heat source considering the Gaussian profile of the laser beam. Figure 6 shows the COMSOL result. Scratch and stay test thermal images are given in annex B, which is similar to the stationary point or plane heat source problem. The temperature rise for the stationary point heat source calculated from equation (1) is 778°C. This is 150°C higher than the thermal softening temperature of silicon [10].

For the moving plane heat source, we have assumed a circular Gaussian profile with the 3μm radius. The temperature rise shown in figures 4 & 5, at velocity of 0.002 mm/sec, is 468°C, which is closer to the estimated

experimental value of 570 °C. The model uses equation 5 with 100 spatial divisions in each of the three direction x, y and z. To evaluate and obtain accurate results, the mesh units (number of spatial divisions) was increased gradually from 20 to 100. As we changed this parameter from 20 to 100 the change in temperature was approximately 50°C. To obtain an accurate estimate one should increase this mesh number in the analytical solution and investigate the temperature rise. The temperature rise in this case is 100°C higher than the thermal softening temperature.

The COMSOL result, for a stationary heat source (comparable to the scratch and stay test results shown in figures 10-15) is shown in figure 6, which gives a temperature rise of 631°C. The COMSOL results are in good agreement with the previous estimated temperature (based upon the measured hardness) of 600°C [3].

the physical properties of Si-II is very limited and there is minimal data available on the absorption of the laser in Si-II [4].

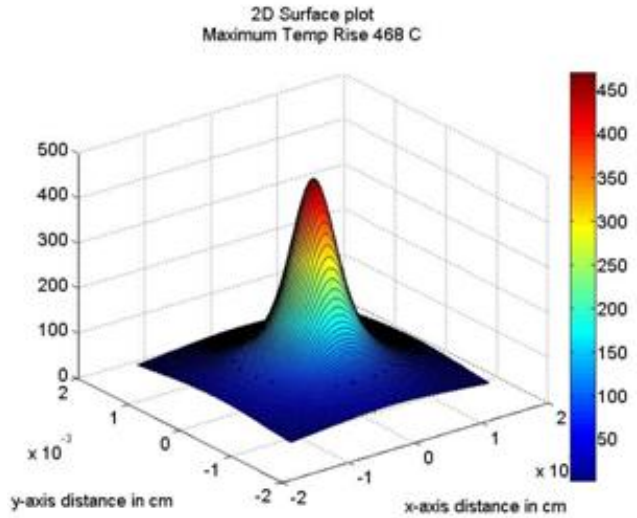


FIGURE 5: 2D SURFACE TEMPERATURE DISTRIBUTION AT 0.002 MM/SEC

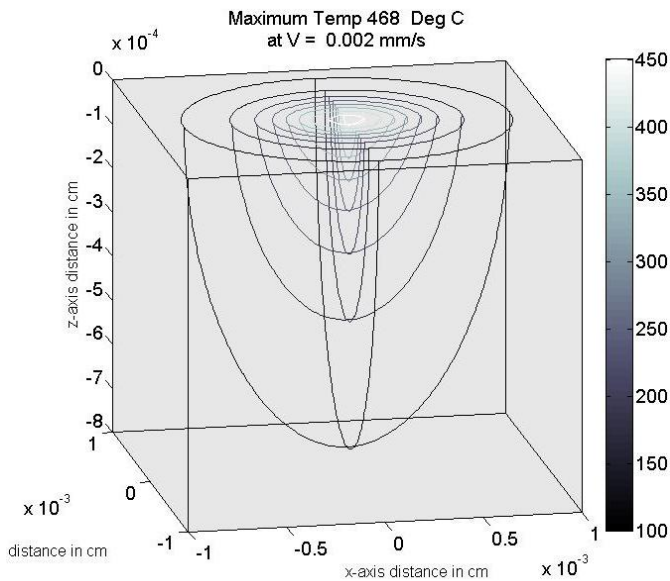


FIGURE 4: 3D TEMPERATURE DISTRIBUTION IN SILICON AT 0.002 MM/SEC

It can be seen from figure 15 (in the appendix-B) that due to the phase change that silicon undergoes, in the area between the covalent silicon and the diamond tool ,shows higher photon energy, which means that the absorptivity of the silicon-II is different than the silicon-I and therefore the temperature rise occurs is due to this HPPT. The FEA results confirm the previous experimental results, wherein 631°C temperature rise occurs with considering room temperature.

7 CONCLUSION

Silicon-II is a metallic high pressure phase of silicon and it is not stable, i.e., it is meta-stable, which makes it difficult to analyze in-situ or post process. Moreover, the availability of

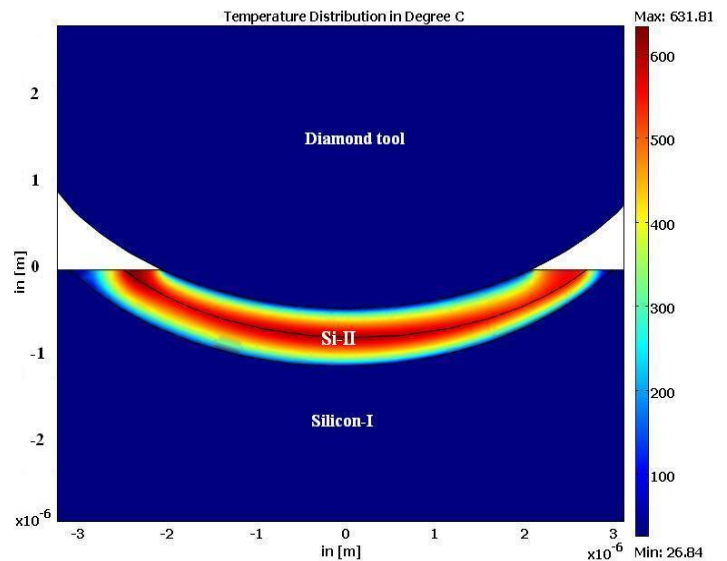


FIGURE 6: TEMPERATURE DISTRIBUTION: COMSOL RESULTS

The reflectance and heat loss reduces the energy absorbed, which reduces the potential temperature rise. According to theoretical calculations the required energy to raise the temperature of silicon would be around 2-9 mW for the experimental conditions considered in this paper [3]. From the visual observation of the IR images it is can be inferred that the silicon directly beneath and in contact with the tool, i.e., the metallic Si-II phase, absorbs the laser energy but the surrounding silicon-I material does not. The resulting

estimated temperature rise is within the range of the softening temperature of silicon (500-800°C) and below the melting temperature. The numerical result and the moving plane heat source with Gaussian beam assumption results are in good agreement with the each other. Moreover, the scratch test results (increased depth of penetration at a fixed load, and thus a reduced hardness, via thermal softening), using laser assisted machining confirm a significant contribution to the temperature rise by the laser.

8 ACKNOWLEDGMENTS

The authors (Suthar and Patten at WMU) wish to acknowledge the financial support of the Michigan Universities Commercialization Initiative (MUCI) grant for 2007-2008 that partially supported the work (thermal modeling) described in this paper.

9 REFERENCES

[1] Abdel-Aal, H. A., Y. Reyes, et al. (2006). "Extending electrical resistivity measurements in micro-scratching of silicon to determine thermal conductivity of the metallic phase Si-II." *Materials Characterization* 57(4-5): 281-289.

[2] Carslaw, H. S. and J. C. Jeager (1953). *Conduction of Heat in Solids*. Clarendon, UK, Oxford.

[3] Dong, L. (2006). In-situ detection and heating of high pressure metallic phase of silicon during scratching. United States -- North Carolina, The University of North Carolina at Charlotte., PhD Dissertation, Mechanical Engineering Dept.

[4] Hanfland, M., M. Alouani, et al. (1988). "Optical properties of metallic silicon." *Physical Review B* 38(18): 12864.

[5] Hou, Z. B. and R. Komanduri (2000). "General solutions for stationary/moving plane heat source problems in manufacturing and tribology." *International Journal of Heat and Mass Transfer* 43(10): 1679-1698.

[6] Komanduri, R. and Z. Hou (2000). "Thermal analysis of the arc welding process: Part I. General solutions." *Metallurgical and Materials Transactions B* 31(6): 1353-1370.

[7] Komanduri, R. and Z. B. Hou (2001). "Analysis of heat partition and temperature distribution in sliding systems." *Wear* 251(1-12): 925-938.

[8] Lide, D. R. (2003-2004). *CRC Handbook of Chemistry and Physics, Student Edition*, CRC Press.

[9] Moody, J. E. and R. H. Hendel (1982). "Temperature profiles induced by a scanning cw laser beam." *Journal of Applied Physics* 53(6): 4364-4371.

[10] Trefilov, V.I., Milman, Y.V., "Sbornik Voprosy Fiziki metallov i metallo-vedeniya", Vol. 17, Izd. Akad. Nauk Ukr.SSR, 45 (1963).

[11] Palik, E.D., *Handbook of Optical Constants of Solids*. 1st ed, ed. E.D. Palik. 1997: Academic Press. 3224. Moody, J..

[12] Engineering, E. & C. *Complex Index of Refraction Look-up Utility*. 2008 [cited 2008 June 15, 2008]; Available from:

<http://www.ee.byu.edu/photonics/opticalconstants.phtml>.

ANNEX A

MOVING POINT HEAT SOURCE MATLAB PROGRAM (TRIBOLOGICAL APPLICATION)

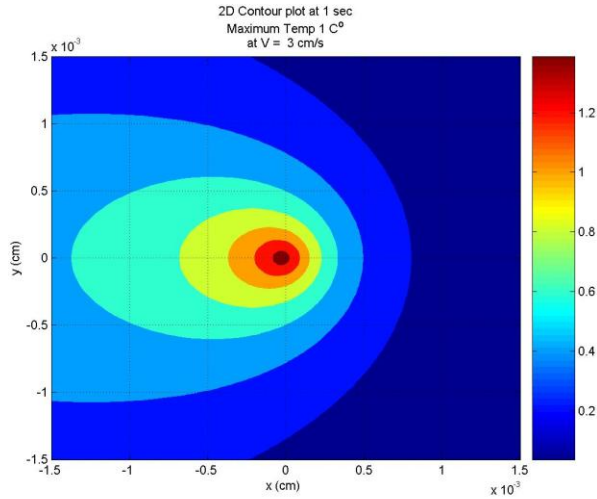


FIGURE 7: MOVING HEAT SOURCE SOLUTION AT 1 SEC AND 3 CM/S VELOCITY

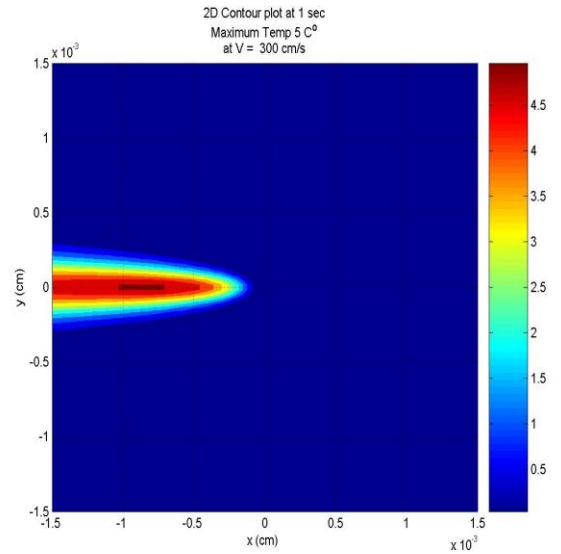


FIGURE 9: MOVING HEAT SOURCE SOLUTION AT 1 SEC AND 300 CM/S VELOCITY

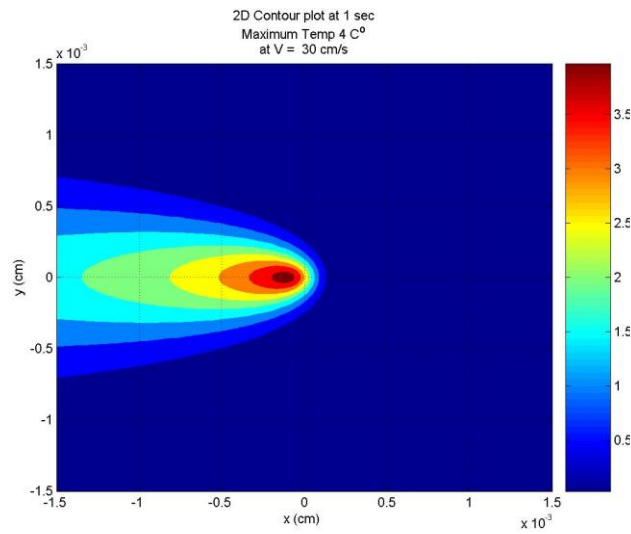


FIGURE 8: MOVING HEAT SOURCE SOLUTION AT 1 SEC AND 30 CM/S VELOCITY

ANNEX B

THERMAL IMAGES

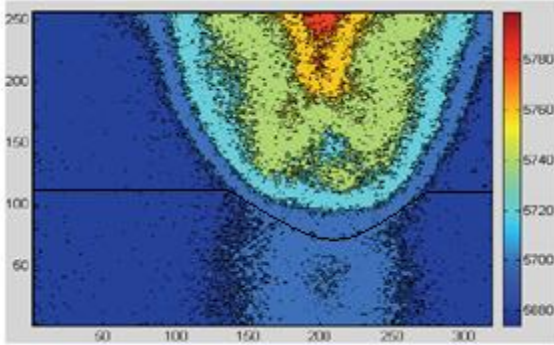


FIGURE 10: THERMAL IMAGE OF THE DIAMOND TIP AND ADJACENT AREA IN THE LAST 5 SECONDS: STAGE-1

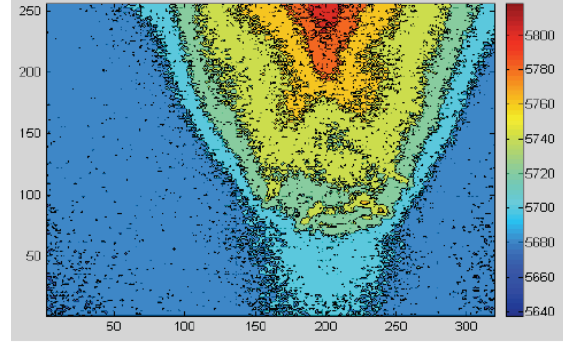


FIGURE 13: THERMAL IMAGE OF THE DIAMOND TIP AND ADJACENT AREA IN THE LAST 5 SECONDS: STAGE-4

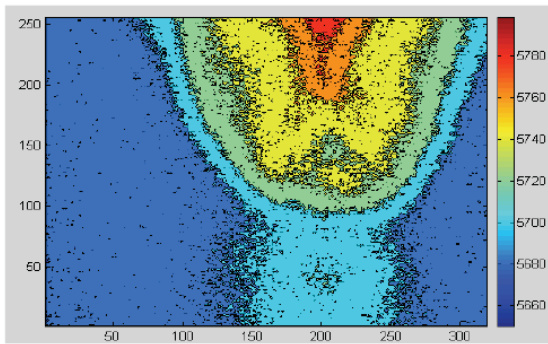


FIGURE 11: THERMAL IMAGE OF THE DIAMOND TIP AND ADJACENT AREA IN THE LAST 5 SECONDS: STAGE-2

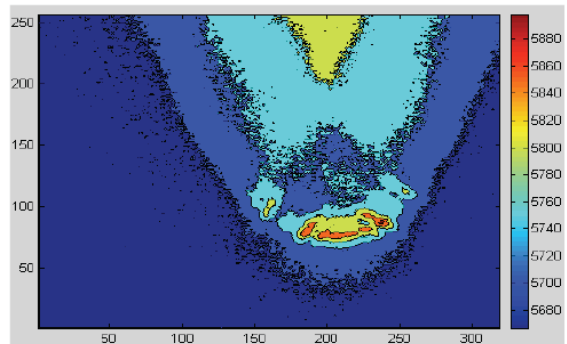


FIGURE 14: THERMAL IMAGE OF THE DIAMOND TIP AND ADJACENT AREA IN THE LAST 5 SECONDS: STAGE-5

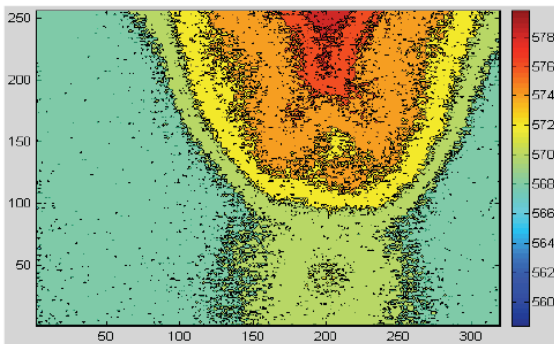


FIGURE 12: THERMAL IMAGE OF THE DIAMOND TIP AND ADJACENT AREA IN THE LAST 5 SECONDS: STAGE-3

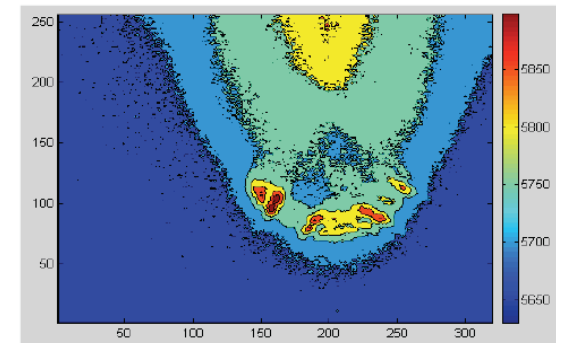


FIGURE 15: THERMAL IMAGE OF THE DIAMOND TIP AND ADJACENT AREA IN THE LAST 5 SECONDS: STAGE-16